Active mechanical metamaterial with embedded piezoelectric actuation

Saravana Jothi, N. S.; Hunt, A.

DOI
10.1063/5.0101420

Publication date
2022

Document Version
Final published version

Published in
APL Materials

APL Materials

Active mechanical metamaterial with embedded piezoelectric actuation

Cite as: APL Mater. **10**, 091117 (2022); https://doi.org/10.1063/5.0101420
Submitted: 31 May 2022 • Accepted: 23 August 2022 • Published Online: 27 September 2022

N. S. Saravana Jothi and A. Hunt

AIP Publishing

Active mechanical metamaterial with embedded piezoelectric actuation

Cite as: APL Mater. 10, 091117 (2022); doi: 10.1063/5.0101420
Submitted: 31 May 2022 • Accepted: 23 August 2022 •
Published Online: 27 September 2022

N. S. Saravana Jothi and A. Hunt[a)]

AFFILIATIONS

Department of Precision and Microsystems Engineering, Delft University of Technology, Mekelweg 2, 2628CD Delft, The Netherlands

Note: This paper is part of the Special Topic on Design, Material, Function, and Fabrication of Metamaterials.
[a)]**Author to whom correspondence should be addressed:** A.Hunt@tudelft.nl

ABSTRACT

Metamaterials are artificially structured materials and exhibit properties that are uncommon or non-existent in nature. Mechanical metamaterials show exotic mechanical properties, such as negative stiffness, vanishing shear modulus, or negative Poisson's ratio. These properties stem from the geometry and arrangement of the metamaterial unit elements and, therefore, cannot be altered after fabrication. Active mechanical metamaterials aim to overcome this limitation by embedding actuation into the metamaterial unit elements to alter the material properties or mechanical state. This could pave the way for a variety of applications in industries, such as aerospace, robotics, and high-tech engineering. This work proposes and studies an active mechanical metamaterial concept that can actively control the force and deformation distribution within its lattice. Individually controllable actuation units are designed based on piezostack actuators and compliant mechanisms and interconnected into an active metamaterial lattice. Both the actuation units and the metamaterial lattice are modeled, built, and experimentally studied. In experiments, the actuation units attained 240 and 1510 μm extensions, respectively, in quasi-static and resonant operation at 81 Hz, and 0.3 N blocked force at frequencies up to 100 Hz. Quasi-static experiments on the active metamaterial lattice prototype demonstrated morphing into four different configurations: Tilt left, tilt right, convex, and concave profiles. This demonstrated the feasibility of altering the force and deformation distribution within the mechanical metamaterial lattice. Much more research is expected to follow in this field since the actively tuneable mechanical state and properties can enable qualitatively new engineering solutions.

I. INTRODUCTION

Increasingly better and specialized engineering materials are required to meet the innovation needs in medicine, aerospace, and many other fields. Metamaterials are man-made materials that are engineered to exhibit properties that are uncommon or absent in nature and differ from the properties of their constituent materials.[1,2] They are achieved by smart design of mesostructures: Functional unit elements are interconnected into a repeating lattice that appears as a continuum material on a macroscale and exhibits a tailored functionality, e.g., altering electromagnetic waves, sound, or mechanical stimuli.[3] Mechanical metamaterials (MM) make use of mechanisms in their unit elements to attain exotic mechanical properties,[1] e.g., negative Poisson ratio, pentamode behavior, and compensation of thermal expansion.[4–6] More complex behaviors can be realized by altering the shape, geometry, orientation, and arrangement of unit elements.[7] While MMs allow for attaining a broad range of properties beyond conventional materials, these properties are permanently fixed by the design.

Active mechanical metamaterials (AMM) can overcome these limitations by embedding sensors and actuators within their unit elements. This allows us to attain central and/or localized control over the distribution of the material properties and/or state within the AMM lattice. Such an approach can achieve significantly broader adjustability in material properties than altering the conventional materials via temperature or other means[8,9] and attain novel properties, such as direct control over the material stress or strain field, controllable stiffness, and increased damping without adding damping material. These properties are realized in lumped mechatronic systems (e.g., haptics[10] and vibration isolation[11]) by actuation and dynamic control but not yet in material volumes. While AMMs can be activated by embedding conventional

transducers (addressable as mechatronic metamaterials), utilization of smart material transducers[12–14] or active composites[15,16] is more promising due to their simpler construction and perspective for additive manufacturing.[17–19]

Integration of actuation into metamaterials has been studied in numerous reports to alter their optical or electromagnetic properties.[20] Embedded actuation in mechanical metamaterial (or similar) structures has been studied only in a few reports. Poon and Hopkins proposed a metamaterial design that consists of a 3D array of Ga-filled silicone cells with integrated heater wires that can melt Ga to change the stiffness of the cells.[21] Reaction time in such a concept is limited by the rate of heat exchange. Overvelde *et al.* proposed an origami-inspired 3D MM that can alter its shape, volume, and stiffness.[22] It consists of rigid faces and pneumatically actuated hinges that form a periodic lattice of extruded cubes and can be actuated in 3 DOFs. Haghpanah *et al.* integrated electromagnets within MM unit cells that can lock or unlock the cell, allowing to individually switch between two cell stiffness to vary the lattice stiffness, Poisson ratio, and buckling strength.[9] Thomas used electromagnets to design MM unit cells that can alter their damping coefficient via electromagnetically altering the Coulomb friction.[23] These solutions cannot input force to alter the dynamic state of the metamaterial[9,23] or are severely limited in bandwidth.[21,22]

To enable dynamic control over the material's stress and strain fields, stiffness, and damping and to attain more advanced functionalities, it is required to embed dynamic actuation in the MM at the unit element level. This paper proposes an approach for designing such active mechanical metamaterials and validates it by designing, building, and studying an AMM prototype. In this approach, the MM is constructed from actuation units by interconnecting them into a MM structure. The actuation units need to provide the stiffness and embedded actuation functionality and must be individually controllable. This work results in the first AMM whose structure is actuated by electric stimulus, therefore, allowing dynamic control over the state of its strain or stress field.

The proposed design approach and rationale to realize the AMM concept are explained in Sec. II A. In this work, the actuation functionality is based on piezoelectric stack transducers (Sec. II A 1). The AMM-specific actuation units are proposed based on the compliant motion amplifier concept, aiming to provide stiffness and mechanical compliance matching between the AMM lattice and the actuator (Sec. II A 2). The actuation units can be connected into a desirable AMM structure, whereas a planar hexagonal lattice is used in this study (Sec. II A 3). The actuation units and the AMM lattices are designed and validated based on analytical and FEM modeling (Sec. II B). First, analytical models of the bridge and rhombus motion amplifiers (Secs. II B 1 and II B 2) are used to design six different actuation units that are further studied using finite element analysis (Sec. II B 3). Next, the best suited actuation unit design is used to build a finite element model of the AMM lattice and further study its functionality in deforming into six different shape profiles (Sec. II B 4). The experimental part of the work (Sec. II C) first builds the prototypes of the best suited actuation unit and the AMM lattice (Sec. II C 1), then studies the force and displacement dynamics of the actuation unit (Sec. II C 2), and finally studies the AMM lattice functionality in producing four different shape profiles (Sec. II C 3). The results and discussion are addressed in Secs. III and IV, and the work is concluded in Sec. V.

II. MATERIALS AND METHODS

To study the proposed AMM concept, the methodology is divided into the design, simulation, and experimental validation parts. Section II A starts with explaining our approach for designing AMMs and then continues on realization, covering the actuator selection, actuation unit design, and AMM lattice design. The modeling in Sec. II B first models the main components of the actuation units analytically, further studies the six actuation unit designs using finite element methods, and finally builds an AMM model from the best actuation unit design and simulates its function in taking six different deformation configurations. The experimental part of this study in Sec. II C first explains the prototyping of an actuation unit and the entire AMM lattice, and then how they are studied, respectively, in dynamic and quasi-static experiments.

A. Active metamaterial design

The AMM design in this study is inspired by the spring-mass (-damper) modeling of material structures, where the material is considered as a network of nodes with a mass, and adjacent nodes are interconnected by vertices with stiffness (and damping). Here, each vertex consists of stiffness, and an embedded actuator for exerting a force between the nodes, allowing control of the local stress or strain states within the material. In this study, these vertices are addressed as actuation units, and the interconnecting nodes as the coupling elements. The main challenges lie in the actuation unit design since they define the stiffness for the AMM structure and must translate the actuator force–displacement profile into the desired output characteristics. This section will first explain the actuator selection in Sec. II A 1, then address the actuation unit design in Sec. II A 2, and finally explain connecting them into an AMM lattice in Sec. II A 3.

1. Actuator

This study used commercially available piezoelectric stack actuators. These transducers are actuated by voltage, exhibit high power densities and bandwidths, and output high forces at small displacements. They are compact and simple in structure (like other smart material actuators), essential for efficient fabrication and miniaturization of the future AMMs. This study selected the SA050520 piezoelectric stack actuator from Piezodrive.[24] It has a footprint of 5×5 mm^2, a length of 20 mm, a weight of 4.0 g, and a stiffness of 41 N/μm. At up to 150 V of operational voltages, it can provide up to 31 μm of actuation range and 900 N of blocking force.

Alternative actuators that were considered for AMM design include electromagnetic, electrostatic, fluidic, thermal, and piezoelectric patch actuators. Compared to the stack transducers that contain a lot of active material in a compact design, piezoelectric patches provide large deflections but are limited in forces and bandwidths. Electrostatic actuators are fast and precise but require very high voltages and produce small deformations.[25,26] Thermal actuators (e.g., bimorphs and Chevrons) produce high forces at low voltages but are limited by heat dissipation. Fluidic actuators allow high energy densities[27] but require bulky controls, and their bandwidth is limited by fluid dynamics. Electromagnetic actuators were excluded due to their poor outlooks in downscaling, i.e., bulky structure and exponential reduction in energy density with size.[28]

2. Actuation unit design

The structural design of the AMM actuation unit needs to translate the actuator functionality into the desired output functionality of the AMM actuation unit. In this study, this means amplifying the limited range of motion of the piezostack actuator (31 μm for the SA050520) while remaining as compact as possible. This is attained by adaptation of the motion amplification mechanisms for mechanical leverage, well known in high-tech engineering.[29] Most feasible mechanisms for designing actuation units of the AMMs are the bridge and rhombus types of motion amplifiers, as explained in Fig. 1.[30] A broader overview of the motion amplifier designs can be found in Ref. 30.

The proposed actuation unit designs use multiple stages of the bridge and rhombus motion amplifiers in series since the single-stage designs cannot simultaneously attain high output stroke and compact design: (1) single-stage designs that can produce large gains and displacements become unreasonably large in size and (2) compact designs remain limited in their range of motion, despite exhibiting very high local gains (see Sec. II B). In multi-stage designs, the total amplification of motion A_m equals the multiplication of the individual stage amplifications $Am_i, i = 1, 2, \ldots, n$, where n is the number of stages,[31]

$$Am = Am_1 \cdot Am_2 \cdot \ldots \cdot Am_n. \quad (1)$$

Besides the transfer of the mechanical energy from the actuators to the mechanism output, a portion of it remains within the amplification mechanism as strain energy, and some of it is dissipated via viscoelasticity. Therefore, the efficiency of the actuation unit is further a trade-off between the material properties and the dimensions of the compliant structures: (1) the materials need to provide sufficient strength, elasticity, and low loss modulus and (2) the compliant mechanisms need to be slender enough to provide low flexural stiffness and remain below the fatigue limit at high strains while being thick enough to bare the stresses.

Actuation unit development investigated two- and three-stage designs based on the motion amplifiers in Fig. 1. In all designs, the bridge amplifier is chosen for the innermost stage since it is much stiffer than the rhombus design and very compact. For the external stage, all the designs use a rhombus motion amplifier since it is less stiff and leaves enough space for inserting the actuator. The two-stage designs differ in the orientation and dimensioning of the amplifiers, while the three-stage designs also vary in the type of the intermediate amplifier stage. The six designs are shown in Fig. 2 and are denoted as follows: (a) a two-stage design that orients both the stages in the same plane; (b) a more compact two-stage design that orients the stages in perpendicular planes; (c) a three-stage design that uses a bridge amplifier for the intermediate stage and places it in the same plane as the inner stage to leave space for actuator placement; (d) another three-stage design with stiffer bridge amplifiers; (e) a three-stage design that uses a rhombus amplifier for the intermediate stage and orients all stages perpendicular to each other; and (f) a more compact version of the previous design.

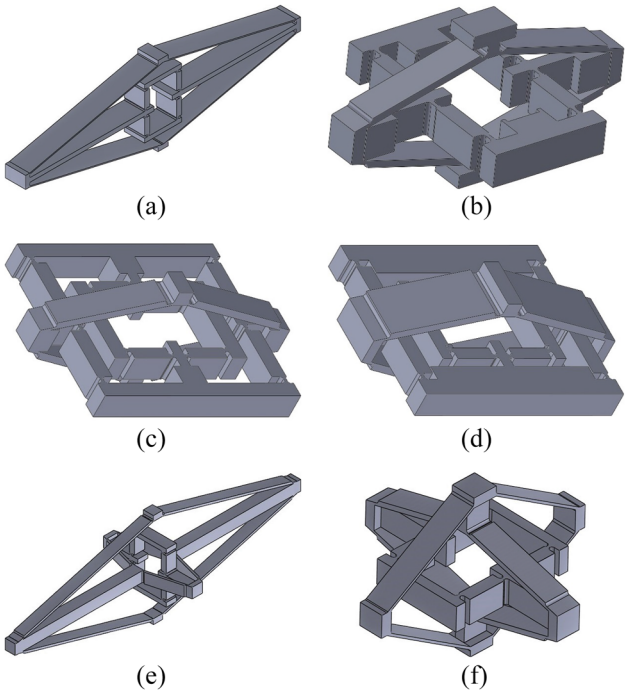

FIG. 2. Actuation unit designs consist of two [(a) and (b)] or three [(c) to (f)] stages of motion amplifiers.

3. Active metamaterial lattice

Based on the actuation unit designs in Sec. II A 2, it is possible to construct a wide variety of planar or three-dimensional AMM lattices. Considering the AMM as a network of nodes (i.e., coupling elements) and vertices (i.e., actuation units), the lattice design is a matter of designing the coupling elements.

This study focuses on a planar design of a hexagonal AMM lattice as shown in Fig. 3. The Y-shaped couplers are interconnected by the actuation units, providing the AMM lattice with its stiffness and actuation functionality. Such AMM design allows local actuation

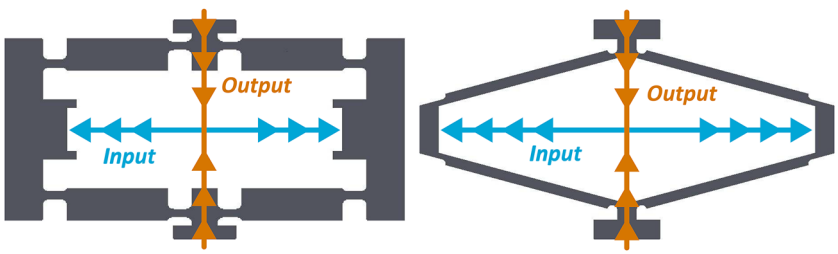

FIG. 1. Motion amplifiers in the actuation unit design: The bridge (left) and the rhombus (right) type.

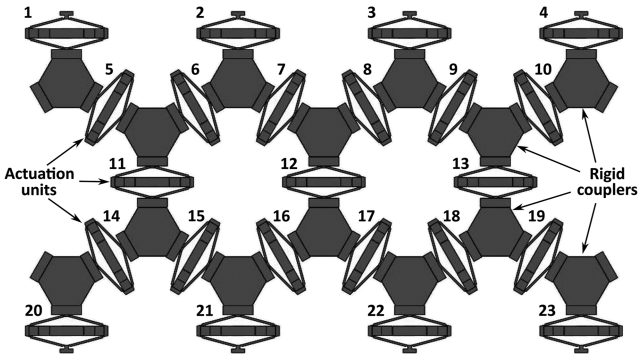

FIG. 3. Interconnecting the actuation units (numbered 1–23) into a hexagonal AMM lattice by the rigid couplers.

of the material lattice within a plane, enabling local (meta)material translations and rotations.

B. Modeling

This section describes the analytical and FEM models that were used in designing and evaluating the actuation units and the AMM lattice design. First, analytical modeling of the bridge and rhombus motion amplifiers is, respectively, given in Secs. II B 1 and II B 2, attaining the dimensions for the mechanism geometries. Next, all the actuation unit designs (Fig. 2) were numerically modeled as described in Sec. II B 3, allowing to account for the design details and study the dynamic behavior. Finally, a FEM model of the AMM lattice was constructed to study actuation in the AMM, as described in Sec. II B 3.

1. Analytical modeling of the bridge amplifier

The operating principle of the bridge amplifier is explained in Fig. 4. Thin and thick geometries in the design function, respectively, as flexible joints and rigid bodies. Elongation of the piezoelectric stack actuator by Δx causes a reduction in the angle α of the segment AB and a further displacement Δy at the output, perpendicular to the Δx direction. Expression for the amplification can be given as[32]

$$Am = \frac{\Delta y}{\Delta x} = 2 \cdot \frac{l_a \sin \alpha - \sqrt{l_a^2 \sin^2 \alpha - \Delta x^2 - 2\Delta x l_a \cos \alpha}}{\Delta x}, \quad (2)$$

where l_a is the length of the motion amplifier linkages. While a compact design requires a small l_a, α can be varied to tailor the amplification. Local motion amplification increases as α approaches 0, and the largest stroke can be attained if $\alpha \approx 0$ occurs at the full extension of the actuator $\Delta x_{\max}$. Then, the maximum displacement can be expressed as[32]

$$\Delta y_{\max} = 2 l_a \sin \alpha. \quad (3)$$

In this case, the length of the linkages that attain the most compact design is $l_a = l_x + \Delta x$, where l_x is the projection of l_a on the x axis, that is, bound by the length of the actuator l_{piezo} such that $l_x \leq 0.5 \cdot l_{piezo}$.

2. Analytical modeling of the rhombus amplifier

The working principle of the rhombus amplifier is explained in Fig. 5. It consists of four thicker bodies at the motion input and output locations and four compliant beams for the amplification mechanism. Motion amplification is described by[33]

$$Am = \frac{\Delta y}{\Delta x} = 2 \cot \alpha, \quad (4)$$

Therefore, it only depends on the beam angles. Again, as α approaches 0, the local motion amplification approaches maximum, while the force transfer approaches 0. Similarly to the bridge amplifier case, choosing the beam angle depends on the maximum input displacement, defined by the previous stage.

3. Finite element modeling of the actuation units

The analytical models in Secs. II B 1 and II B 2 aim for a combined motion amplification of 10× when connecting the two designs in series [Eq. (1)]. Similarly, three-stage configurations are expected to provide more amplification at the cost of lower force transmission. FEM modeling was performed in Comsol Multiphysics 5.6 to

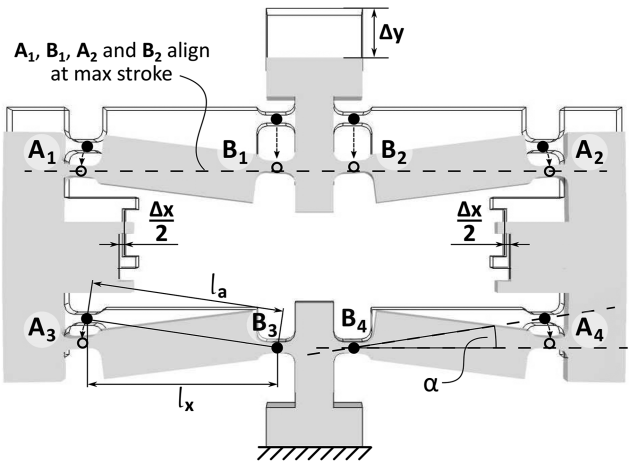

FIG. 4. Modeling the bridge type of motion amplifier: The structure, deformations, and parameters.

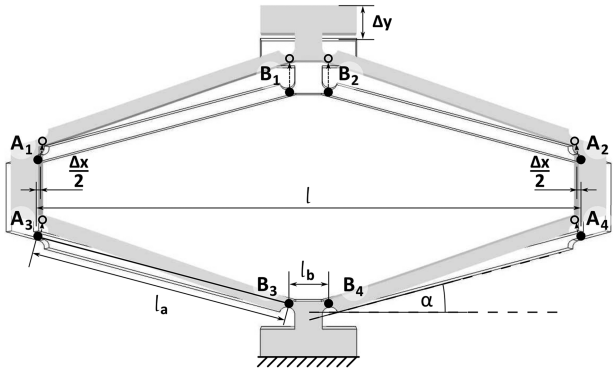

FIG. 5. Modeling the rhombus motion amplifier: The structure, deformations, and parameters.

refine that estimation by accounting for the exact realization of the design and the higher order effects caused by the geometry features and material behavior that were omitted in the analytical models.

In this modeling study, the six actuation unit designs in Fig. 2 (Sec. II A 2) were investigated under free displacement conditions to estimate their extension under static loading. One end of the actuation unit was fixed as a boundary condition, and the displacement of the other end was measured in the simulations. The actuation input was modeled as a constant displacement of 31 μm, which is equal to the maximum actuation range specified for the SA050520 actuator. The designs were evaluated by their output displacements and structural deformations, and the best-performing actuation unit was further analyzed under dynamic excitation using the same displacement amplitude within the frequency interval of 1–500 Hz.

4. Modeling the lattice

Evaluating the proposed design of the AMM lattice was performed in Comsol Multiphysics 5.6. The model was built in SolidWorks 2019, and it consisted of 23 actuation units and 14 rigid couplers. The resulting model configuration and meshing are shown in Fig. 6. Actuation of the AMM was simulated by providing displacement inputs at the intended piezostack locations within the actuation units. Due to the limited amount of available actuators in the experimental phase (see Sec. II C 1), the AMM model was only activated at up to six actuator locations in the first four simulations, while the remainder of the actuator locations were left unconstrained. This allowed for matching the simulation conditions to the respective four experiments in Sec. II C.

The simulations studied various quasi-static deformations that the AMM lattice design can attain. The bottom row of the actuation units was fixed to the Earth frame, and the populated actuation units were activated, aiming to produce the following six behaviors at the top row of the actuation units: (1) tilt to the right using the actuation units 1, 5, 11, 14, and 20; (2) tilt to the left using the actuation units 4, 10, 13, 19, and 23; (3) concave profile by activating the actuation units 1, 4, 11, 13, 20, and 23; (4) convex profile by activating the actuation units 2, 3, 12, 21, and 22; (5) piston motion in the vertical direction by activating actuation units 1, 2, 3, 4, 11, 12, 13, 20, 21, 22, and 23; and (6) uniform expansion via activating all the actuation units. In the first four simulations, the activate actuation unit locations were initially varied to identify the best placement for maximum output. The fifth and sixth behavior were only simulated and not studied in the subsequent experiments.

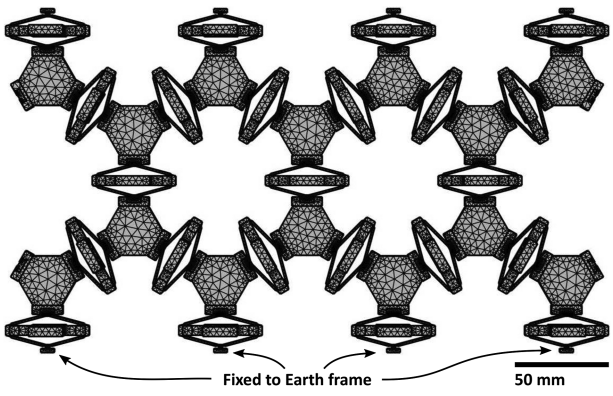

FIG. 6. Comsol model of the AMM lattice.

C. Experimental

For experimental validation of the proposed AMM concept, the actuation unit and AMM lattice prototypes were first constructed, as explained in Sec. II C 1. Furthermore, Secs. II C 2 and II C 3 describe the experimental set-ups and methodology, respectively, for studying the dynamic behavior of the individual AMM actuation unit and for studying the deformation profiles that the AMM lattice prototype can attain.

1. Actuation unit and AMM prototypes

The AMM actuation units were manufactured from a thermoset acrylic resin (Stratasys Vero[34]) on a Stratasys Polyjet J735 3D printer. This allowed for attaining the motion-amplifying structures in a single print, at roughly homogeneous material properties. Piezoelectric stack actuators (SA050520, see Sec. II A 1) were placed into the motion-amplifying structures to make the actuation units active. In the actuation unit dynamics measurements (Sec. II C 2), the actuator was further bolted in place to prevent it from decoupling during the high-frequency excitation. An assembled actuation unit is shown in Fig. 7.

The AMM lattice prototype was constructed according to the design explained in Secs. II A 3 and II B 3 and in Fig. 3. The active and passive actuation units were interconnected into a lattice structure using the Y-shaped couplers and fixed to the Earth frame at the bottom row using the mounting modules. Using slide-in connectors at all of the interconnections made the design modular for fast design alterations and servicing. All these additional components were 3D printed from PLA on a Prusa i3 MK3, and the resulting prototype is shown in Fig. 11.

2. Measuring the actuation units

Experiments on the actuation units measured their quasi-static and dynamic responses under the free displacement and blocked force conditions. The experimental setup for these measurements is

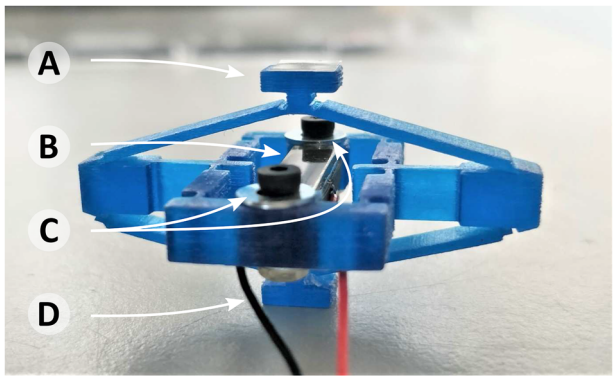

FIG. 7. An AMM actuation unit with an integrated piezoelectric actuator. (a) output node, (b) piezoelectric stack actuator, (c) fasteners to support the actuator, and (d) fixed node.

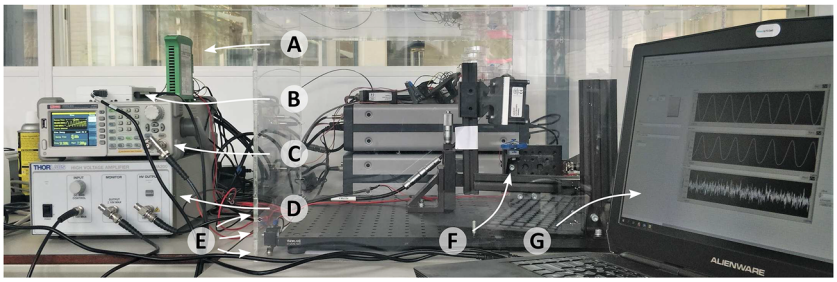

FIG. 8. Experimental setup for studying the AMM actuation unit. (a) strain gauge amplifier, (b) NI USB-6211 data acquisition board, (c) waveform generator, (d) high voltage amplifier, (e) acrylic protective enclosure, (f) actuation unit and sensors for displacement and force measurements, and (g) PC with NI LabVIEW 2018 environment.

shown in Fig. 8 and the block diagram in Fig. 9. The following will explain the procedure for these experiments.

In free displacement experiments, the actuation unit was attached to one end to the Earth frame, and a laser displacement sensor (optoNCDT 1750-2, Micro-Epsilon, range 2 mm, resolution 0.1 μm) was used to measure the displacement of the output in the free end, as shown in Fig. 10. The driving signals were produced by an RS Pro RSDG 805 arbitrary waveform generator (AWG) and applied to the piezoelectric actuators via a Thorlabs HVA200 high voltage amplifier. The monitor line output of the HVA200 amplifier (i.e., the voltage on the actuator) and the output of the laser displacement sensor were routed to a NI USB-6221 data acquisition card, which was connected to a PC computer with NI LabVIEW 2018 environment, as shown in Figs. 8 and 9. The entire setup was placed in a transparent acrylic chamber for safety.

The blocked force experiments were conducted on a similar set-up, differing in the clamping conditions and the sensor: The output end of the actuation unit was attached to a force sensor (Futek LSB200), as shown in Fig. 10. Force sensor output was connected to the NI USB-6221 data acquisition board input, in place of the laser displacement sensor (see Fig. 9). The other end of the force sensor was fixed to the Earth frame, allowing it to measure the actuation force and restrict any motion.

In free displacement configuration, the quasi-static experiments measured the voltage–displacement curves of the actuation units, and the dynamic experiments measured their frequency responses. In the frequency response measurements, the piezoelectric stack actuators were excited by a 1–500 Hz logarithmic chirp signal with a 75 V amplitude, 75 V offset (i.e., 0–150 V), and 50 s duration. In the voltage–displacement measurements, the same excitation amplitude and offset were used at a 1 Hz frequency. This resulted in an input displacement range of ~25.8 μm. The voltages that were applied to the actuator (i.e., at the monitor output) and the output of the laser displacement sensor were read and recorded in a file by a LabVIEW program for the whole duration of the experiments. The data were processed and plotted in Matlab 2021 environment, using the "tfestimate" and "mscohere" functions to extract the Bode and coherence plots.

Similar experiments were conducted in the blocked force configuration to measure the voltage–force curve and the frequency response of the actuation force. As a major difference, the frequency response measurements of the actuation force used a 20 s long chirp signal in the 1–100 Hz interval for excitation. The narrower frequency range was used since the actuation units started to crack at higher frequencies.

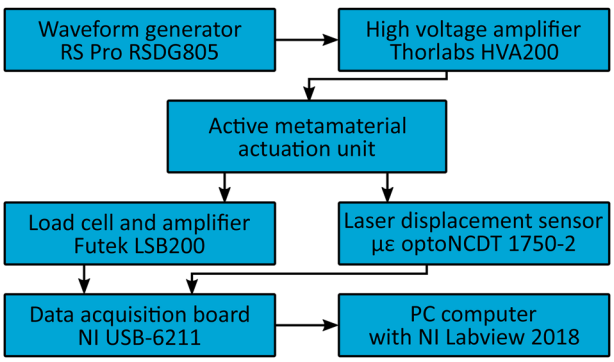

FIG. 9. Block diagram of the experimental set-up for measuring the actuation unit displacements and forces.

3. Experiments on the AMM lattice

Experiments on the AMM lattice aimed to validate their functionality by producing the same displacement profiles as the first four simulations in Sec. II B 4 (tilt left, tilt right, concave profile, and convex profile). Due to the limited availability, only up

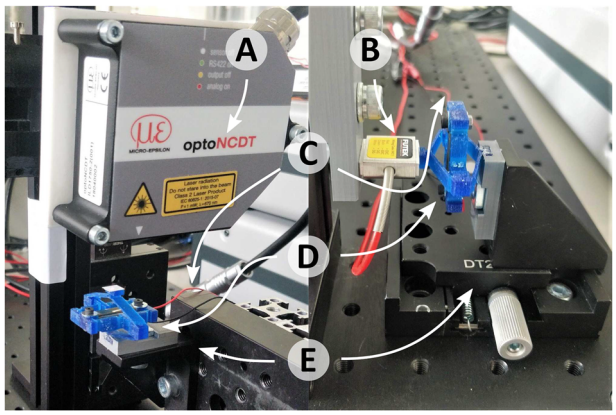

FIG. 10. Actuation unit in the displacement (left) and force (right) measurements. (a) laser distance meter, (b) load cell, (c) wires for powering the actuation unit, (d) actuation unit, and (e) manual XY stages for positioning and fixing the actuation unit.

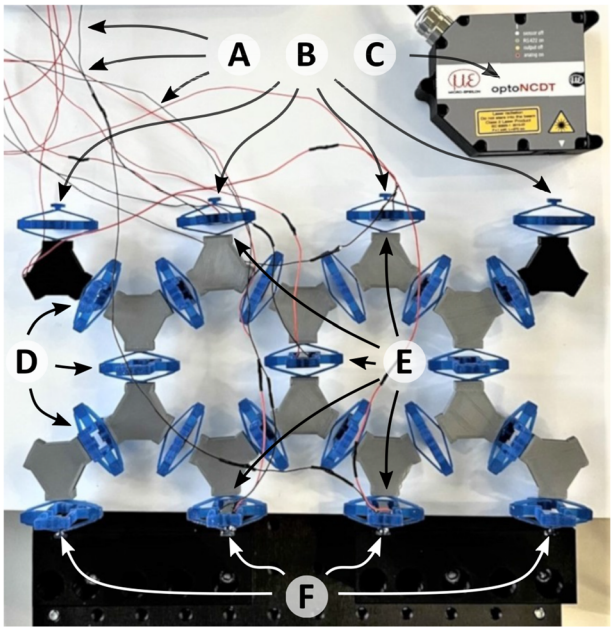

FIG. 11. Experimental setup for measuring the AMM lattice deformations currently set up for convex profile measurements at node 4 location. (a) Wires for powering the actuation units, (b) measurement locations, (c) laser displacement sensor, (d) unwired actuation units remain inactive, (e) active actuation units are wired, and (f) bottom row is fixed to the Earth frame.

to six actuation units were populated with the piezoelectric actuators (SA050520), using the same configuration as simulations (1) through (4).

In the experiments, the bottom row of the AMM lattice was fixed to the Earth frame using 3D-printed mounts (PLA, Prusa i3 MK3), as shown in Fig. 11. The displacement profile at the top row of the AMM prototype was measured using an optoNCDT 1750-2 laser displacement sensor (Micro-Epsilon). The actuators were electrically connected in parallel and driven by an RS Pro RSDG 805 AWG via a Thorlabs HVA200 amplifier, similarly to the actuation unit measurements in Sec. II C 2.

The active actuation units were excited by a sinusoidal signal with a 75 V amplitude, 75 V offset (i.e., 0–150 V), and 0.1 Hz frequency. The cyclic motion of each node was measured in separate experiments, by moving the displacement sensor to a new location between the experiments. Voltage and displacement were read and stored by a LabVIEW 2018 program in a PC computer via a NI USB-6221 data acquisition board. The results were processed and compared against the simulation data using Matlab 2021.

III. RESULTS

This section presents the results of studying the proposed AMM concept. First, the modeling of the actuation units and the metamaterial lattice prototype are addressed in Sec. III A, and then, the respective experimental results are presented in Sec. III B.

A. Modeling

Modeling was performed as described in Sec. II B. In the following, the results are first given for the analytical modeling of the bridge and rhombus motion amplifiers in Sec. III A 1, then for the modeling of the actuation units using FEM in Sec. III A 2, and finally for the AMM lattice prototype in Sec. III A 3.

1. Motion amplifiers

The results for analytical modeling of the bridge and rhombus amplifiers (Secs. II B 1 and II B 2) are shown in Fig. 12, indicating how their motion amplification factors and actuation ranges vary for different beam angles in the design. These results are based on the dimensions and the stroke of the SA050520 actuator (Sec. II A 1). To attain the combined motion amplification of 10×, the beam angles of 8.5° and 17.8° were chosen, respectively, for the bridge and rhombus designs. This allows us to accommodate the entire displacement range of the bridge amplifier and leaves enough space for actuator installation, given that these stages are placed in perpendicular planes.

2. Actuation units

FEM modeling of the actuation unit designs (see Sec. II A 2 and Fig. 2) was performed according to Sec. II B 3. Deformation heat maps for the actuation units upon a 31 μm input displacement are

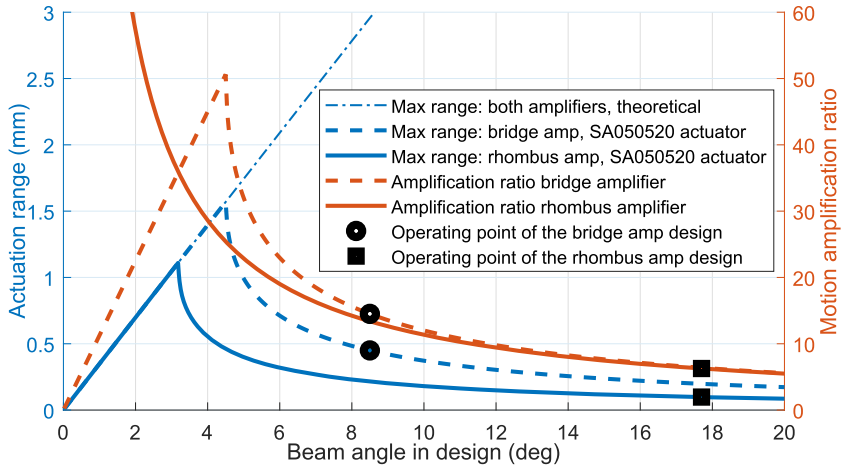

FIG. 12. Actuation ranges (left axis) and motion amplification ratios (right axis) according to the bridge and rhombus amplifier models. Estimations are given based on the SA050520 piezostack actuation range (31 μm). Operating points indicate the design angles of the bridge (8.5°) and rhombus (17.7°) amplifiers in this study.

shown in Fig. 13, and the following presents the modeling results for all the designs.

Studying the two-stage actuation units showed that design (a) attains output displacements of up to 287 μm [Fig. 13(a)], meaning a motion amplification factor of 9.26×, very close to the 10× design goal. Simulations further indicated that the long and slender flexures in this design buckle significantly, making this design unfavorable, especially for dynamic operation. The more compact design (b) yielded 307 μm displacements upon the same stimulation [Fig. 13(b)], meaning a 9.90× amplification, and exhibited significantly less buckling due to the shorter flexural structures within the design.

The three-stage actuation units (c) and (d) use bridge amplifiers for the intermediate stage. Design (c) resulted in the output deflection of 200 μm, i.e., 6.45× amplification. Such a low factor was caused by the significant deformations within the intermediate motion amplifier stage, where the intended rigid portions of the design flexed under the load [see Fig. 13(c)]. Design (d) aimed to overcome this flaw by providing adequate thickness at the unwanted deformation sites, achieving a 230 μm displacement output, i.e., 7.42× amplification. Although an improvement, this is less than the simpler two-stage designs (a) and (b) attained.

The three-stage designs (e) and (f) use rhombus amplifiers for the intermediate stage. The design (e) achieved a maximum displacement of 872.5 μm, meaning an amplification factor of 28.14× [Fig. 13(e)]. While this is roughly three times more than in the designs (a) and (b), the dimensions increase from 46 to 146 mm since the gains >3× require beam angles <15° (Sec. II B 2). The size and buckling make this design impractical. To achieve a more compact actuation unit, the beam angles were varied in simulations between 15° and 45°. This resulted in the design (f) that attained displacements of 286.68 μm, i.e., 9.24× amplification [Fig. 13(f)]. Therefore, no performance improvement was achieved over the design (b) once the dimensions were made similar.

The best amplification-to-size ratio was attained by the design (b), and it was further used as the actuation unit in the AMM lattice. In all simulations, the von Mises stresses remained well below the yield strength of the Vero material (65 MPa), resulting in no plastic deformations.

3. AMM lattice

The AMM lattice design (Sec. II A 3) was simulated as described in Sec. II B 4, and the results are graphically depicted in Fig. 14. The following addresses the simulated deformation configurations in accordance with the numbering of Sec. II B 4: (1) Tilt to right in Fig. 14(a) produced a 0.25° rotation angle as the top leftmost node of the lattice was displaced vertically by 1.07 mm and the rightmost node by −0.183 mm. (2) Tilt to the left in Fig. 14(b) attained identical results in the opposite direction due to the symmetrical design. (3) Concave profile in Fig. 14(c) was attained by producing a vertical displacement between the outer (i.e., nodes 1 and 4) and the

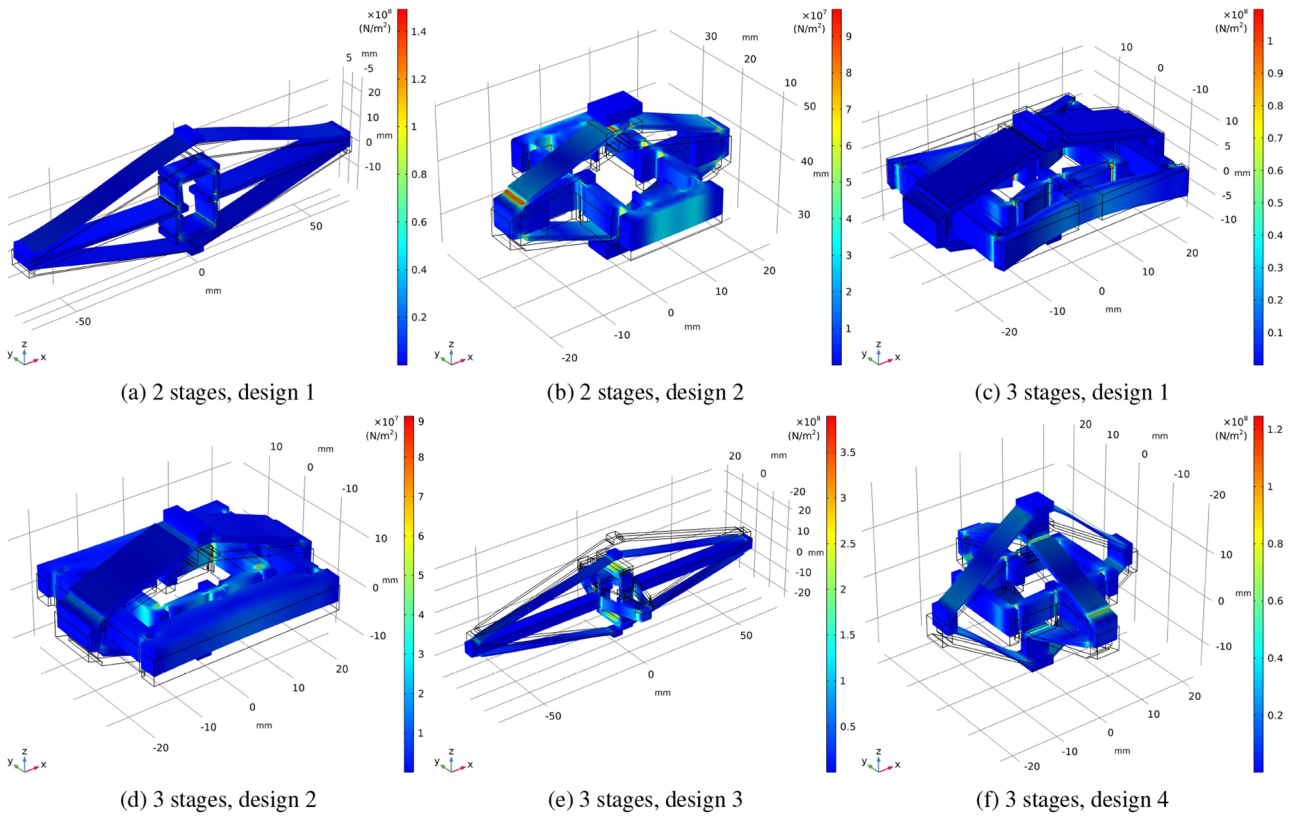

(a) 2 stages, design 1 (b) 2 stages, design 2 (c) 3 stages, design 1

(d) 3 stages, design 2 (e) 3 stages, design 3 (f) 3 stages, design 4

FIG. 13. Finite element analysis of the six actuation unit designs showing their deformations and von Mises stresses.

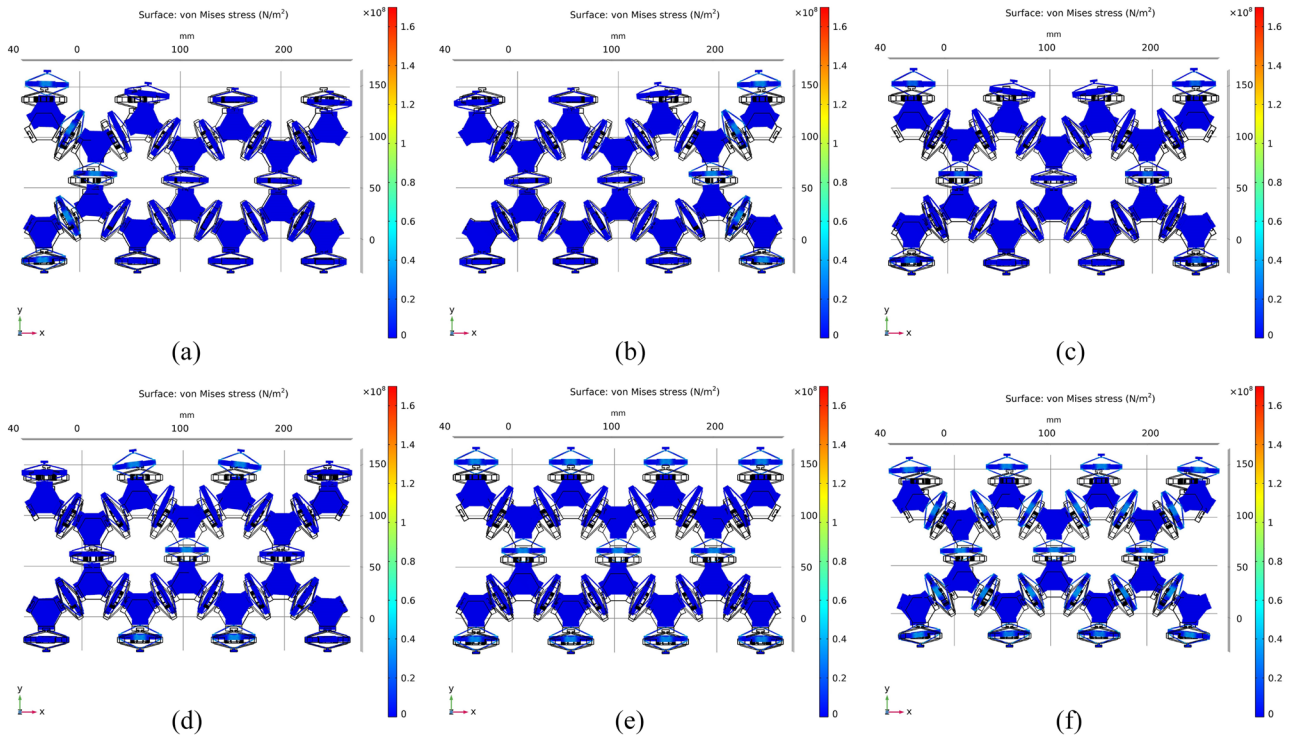

FIG. 14. Simulation results for the AMM lattice taking the six different deformation configurations. (a) Tilt to the right. (b) Tilt to the left. (c) Concave profile. (d) Convex profile. (e) Piston motion. (f) Uniform expansion.

inner nodes (i.e., nodes 2 and 3) of the top row. The vertical displacements of the outer and the inner nodes were, respectively, 0.70 and 0.24 mm. (4) Convex profile in Fig. 14(d) was produced by using the opposite strategy, i.e., by increasing the vertical displacement between the middle and the outer nodes. The resulting vertical displacements were 0.67 and 0.20 mm, respectively. (5) The piston motion showed a 0.87 mm displacement at all of the output nodes. (6) The uniform expansion in Fig. 14(f) achieved the maximum vertical displacement of 1.14 mm upon activation of all the 23 actuation units.

B. Experimental

Experiments were conducted according to the procedure described in Sec. II C. In the following, the results are first given for the actuation unit measurements in Sec. III B 1 and then for the experiments on the AMM lattice prototype in Sec. III B 2.

1. Actuation unit

The actuation units were constructed as described in Sec. II C 1 and studied under quasi-static and dynamic excitation as explained in Sec. II C 2. Upon quasi-static excitation (1 Hz, 150V_{pp}, ~26 μm input), the actuation units achieved up to 240 μm displacements, i.e., an amplification factor of 9.29×. Their measured and simulated displacements and forces are plotted in Fig. 15. Some deviations between the simulation and experiment results are observed due to the presence of hysteresis and non-linearity in gain.

Results for the dynamic displacement measurements are given in the Bode and coherence plots in Fig. 16, along with the respective simulation data. In the proportional gain region (up to ~50 Hz), the actuation unit shows ~240 μm displacements, i.e., 9.29× amplification. The first resonance is observed at 81 Hz, exhibiting a maximum displacement of 1510 μm. This is followed by an antiresonance at 111 Hz, forming a pole–zero pair (180° dip followed by a recovery in the phase). The second resonance is observed at 444 Hz with an amplitude of 346 μm. The simulations effectively predicted these resonances, while the exact magnitudes and frequencies somewhat deviate.

Frequency response measurements for the actuation unit force are given in Fig. 17, indicating a roughly constant force output of 0.3 N over the entire range of measurement frequencies.

2. Active metamaterial lattice

The prototype of the AMM lattice was constructed according to Sec. II C 1 and is shown in Fig. 11. The four experiments for measuring the AMM lattice deformation profiles were conducted according to Sec. II C 2. The results are plotted in Fig. 18, showing the motion of the four output nodes alongside the respective simulation results. The maximum displacements for all four experiments and six simulations are summarized in Table I. Discrepancies between the experiments and simulations are primarily caused by the viscoelastic properties of the actuation unit structure.

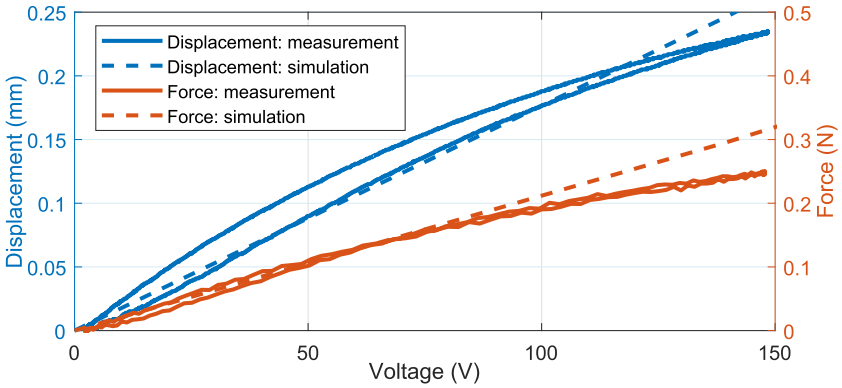

FIG. 15. Displacement and force responses of the actuation unit. Simulation and experimental results upon a 1 Hz sinusoidal excitation at 150 V amplitude.

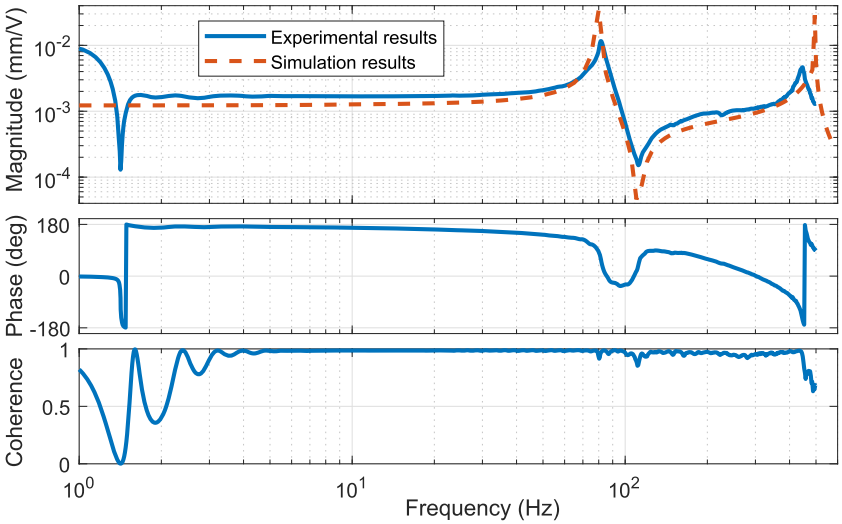

FIG. 16. Bode plots and coherence for the actuation unit free displacement dynamics measurements. The magnitude plot also shows the simulation results for comparison.

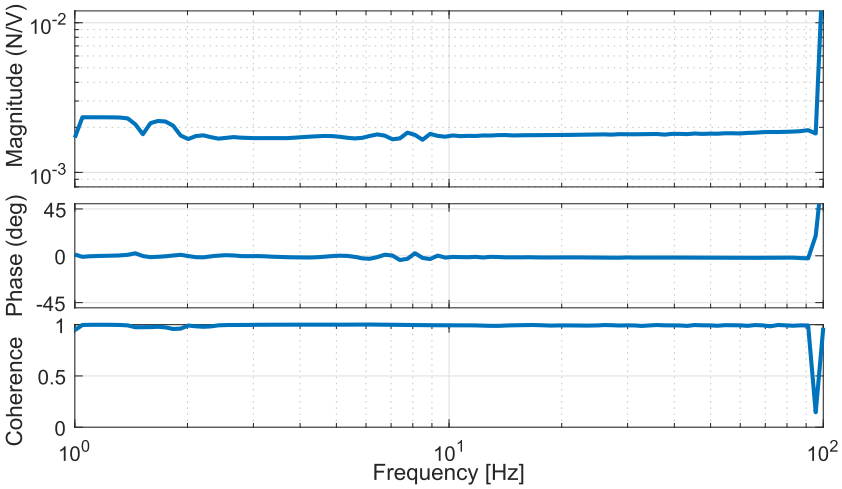

FIG. 17. Bode plots and coherence for the actuation unit blocked force dynamics measurements.

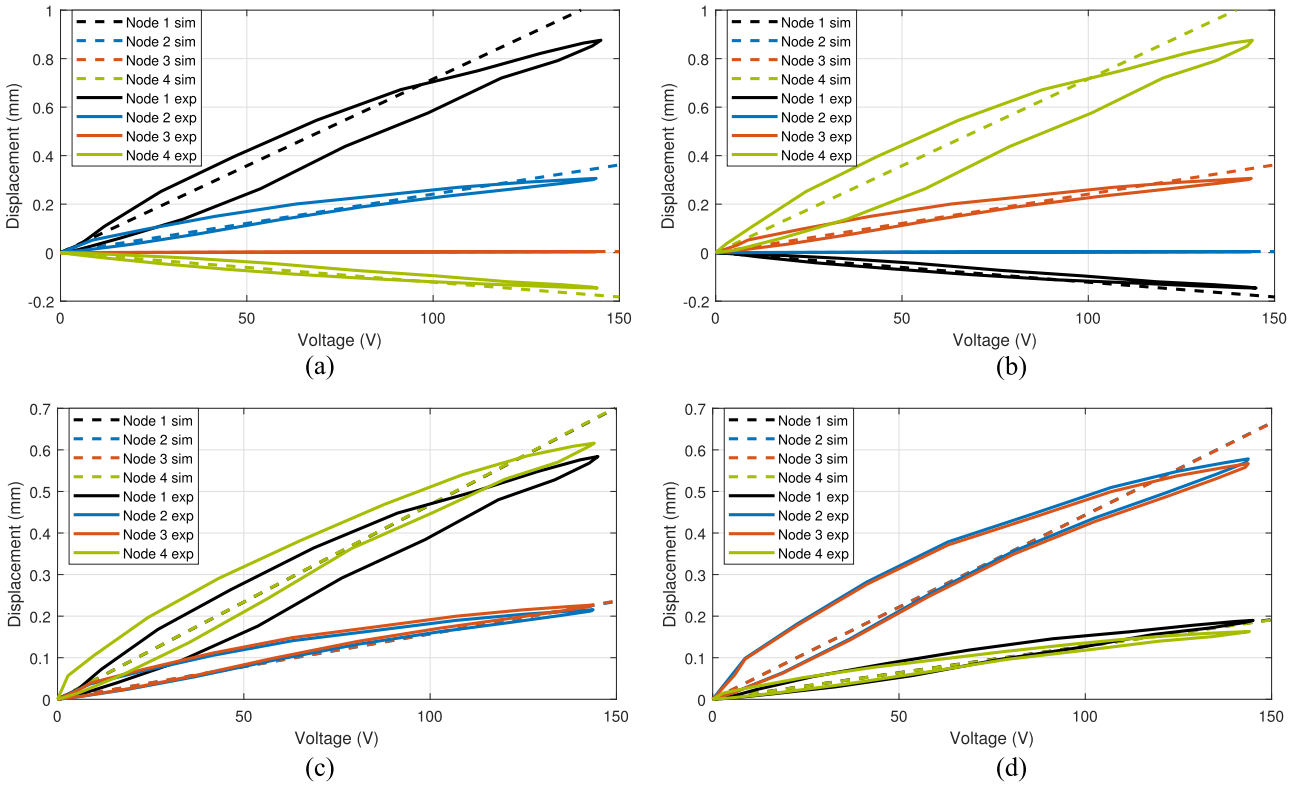

FIG. 18. Results for the AMM lattice experiments (exp) and simulations (sim) of taking four different deformation configurations. The plots show how the four nodes in the top row of the AMM lattice (see Fig. 3) vertically translate upon the application of voltage. (a) Tilt to the right. (b) Tilt to the left. (c) Concave profile. (d) Convex profile.

IV. DISCUSSION

This work proposed and studied a novel concept of active mechanical metamaterials that attain active control over the material configuration and dynamic state. The concept based on the individually driven actuation units that can be interconnected into a lattice to form a metamaterial. Both the actuation units and an AMM lattice were designed, modeled, built, and experimentally studied in this work.

The actuation units in this study are based on the rhombus and bridge type of motion amplifiers. While these structures proved versatile, the AMM design space is open to virtually any mechanism type that can transmit the actuation input from the piezoelectric actuators to the AMM lattice, convert the forces and displacements to the proper range, and provide structural stiffness. Two- and three-stage actuation unit designs were studied in simulations, aiming for a 10× motion amplification. Among the analyzed structures, a two-stage design [Fig. 2(b)] was found to be the most suitable for the purpose of this study. Three-stage designs [Figs. 2(c)–2(f)] performed inferior in simulations, and attaining higher motion amplification proved to be more challenging. This is mainly caused by the undesired deformations that occur in the structural material (Vero) due to its limited stiffness.

Experiments on the chosen actuation unit design showed a good agreement with the simulations: The amplification factor of 9.29× is very close to the 10× target. Minor deviations were observed in the peak gains and resonant frequencies. These are hypothesized to be caused by (1) imperfections in the 3D printed structures of the actuation unit, e.g., variations in the finite voxel sizes and curing, (2) coupling between the actuation units and the actuators, e.g., from the surface roughness and the weak pre-tension, (3) inaccuracies in

TABLE I. Vertical displacements for the nodes in the top row of the AMM lattice: Simulation and experimental results.

	Node displacements (mm)			
Configuration\node	No. 1	No. 2	No. 3	No. 4
Tilt left: Simulation	1.074	0.362	0.005	−0.183
Tilt left: Experiment	0.876	0.306	0.004	−0.146
Tilt right: Simulation	−0.182	0.005	0.362	1.074
Tilt right: Experiment	−0.146	0.04	0.306	0.876
Concave: Simulation	0.702	0.236	0.237	0.703
Concave: Experiment	0.584	0.216	0.226	0.616
Convex: Simulation	0.192	0.665	0.665	0.191
Convex: Experiment	0.190	0.578	0.567	0.163
Piston: Simulation	0.866	0.865	0.865	0.866
Expansion: Simulation	1.043	1.312	1.312	1.042

the material parameters and model, e.g., in the storage and loss moduli, and (4) simplified actuation model that assumes a proportional voltage–displacements relation and neglects the hysteresis. Design, materials choice, and structural optimization of the actuation units require further investigation in future work.

The proposed AMM concept was studied based on the hexagonal lattice configuration, providing sufficient space for the actuation units. Alternatively, they can be interconnected into any lattice configurations (e.g., triangular and rectangular), and enabling the actuation can be selective, i.e., using passive units at the locations where the actuation is not desired. Such selective actuation placement was used in all four experiments on the AMM lattice prototype, and the results matched well with the respective simulations. The minor deviations can be explained by the same reasoning as given above for the actuation unit results and by the Coulomb friction between the AMM prototype and the table that supported it. This support was needed due to the limited stiffness of the 3D printed material. For the same reasons, only the quasi-static experiments were conducted. Future work will address these limitations by using metal structures to attain the required stiffness.

Therefore, the proposed AMM concept was successfully validated both in simulations and experiments, proving it feasible to directly and dynamically control the deformation configuration of a (mechanical meta) material via embedded electromechanical actuators. This further opens the possibility to locally render and alter virtual properties of whole surfaces or volumes of material, as it is possible in lumped mechatronic systems (e.g., haptics[10] and vibration isolation[11]). This sort of AMM concept is expected to enable specialized high-tech materials that are required in industrial applications, such as deformation correction, vibration suppression, and continuum robotic manipulators.

The main challenges toward the mature AMMs were seen to lie in (1) developing actuation solutions that are easy to fabricate, miniaturizable, and have low losses in energy transfer, (2) designing actuation units that efficiently interface the mechanical impedance of the actuator to the desired force–displacement characteristic on the AMM lattice while providing sufficient stiffness, (3) embedding sensing to enable the more exotic material properties that require closed-loop control, and (4) establishing a system integration strategy to manage the wiring and embedded electronics in realizing the local and global control methods. While production actuators were used in this study, in the future, the AMMs are expected to be fabricated by concurrent additive manufacturing of structural material and smart material actuators and/or sensors.[17–19] Developing such materials and techniques is the main focus of our ongoing research.

V. CONCLUSION

This work proposed and created the first active mechanical metamaterial whose unit structures are actuated by electric stimuli. This allows direct and dynamic control over the state of the stress or strain field within the material. The metamaterial architecture is based on actuation units with embedded piezoelectric actuators that are interconnected into a lattice to form a metamaterial, allowing for the application of electrically controllable local actuation within the AMM lattice. Besides the demonstrated shape-morphing functionality, such AMMs will enable in the future to locally render and alter virtual mechanical properties of the whole material surfaces or volumes, similarly to the lumped systems in today's haptics applications.

Six different actuation unit configurations were designed based on the compliant motion amplifier concept and then evaluated in finite element simulations. Force and displacement dynamics of the best actuation unit design were experimentally studied. Free displacement measurement results showed steady-state deflections of 240 μm and peak displacements of 1510 μm for the first resonance at 81 Hz. Blocked force measurements showed that the actuation unit delivers 0.3 N force amplitude over the entire measurement range (up to 100 Hz). Metamaterial was constructed by connecting the actuation units into a planar hexagonal lattice. In simulations and experiments, the bottom row of the lattice was fixed, and the top row successfully demonstrated morphing into four different configurations: Tilt to the left, tilt to the right, convex, and concave profile.

Therefore, the first evidence of the feasibility of the proposed AMM concept was successfully demonstrated. Key challenges toward mature AMMs were seen in developing suitable actuation solutions, designing AMM-specific actuation units, embedding sensing in the AMM structure, and system integration to manage control complexity. Future work will address optimization of the actuation unit designs, reducing losses within the structural material, accounting for the actuator dynamics, and developing the AMM lattice for dynamic operation. The exploitation of such mechatronic materials in applications will require attaining high performance and low costs. This may become possible with the advances in additive manufacturing of smart material transducers, when it becomes possible to print these sensors and actuators concurrently with structural material.

AUTHOR DECLARATIONS

Conflict of Interest

The authors have no conflicts to disclose.

Author Contributions

N. S. Saravana Jothi: Conceptualization (equal); Data curation (equal); Formal analysis (equal); Investigation (equal); Methodology (equal); Validation (equal); Visualization (equal); Writing – original draft (equal); Writing – review & editing (equal). **A. Hunt**: Conceptualization (equal); Data curation (equal); Formal analysis (equal); Investigation (equal); Methodology (equal); Resources (equal); Supervision (equal); Validation (equal); Visualization (equal); Writing – original draft (equal); Writing – review & editing (equal).

DATA AVAILABILITY

The data that support the findings of this study are available from the corresponding author upon reasonable request.

REFERENCES

[1] K. Bertoldi, V. Vitelli, J. Christensen, and M. van Hecke, "Flexible mechanical metamaterials," Nat. Rev. Mater. **2**, 17066 (2017).

[2] R. S. Kshetrimayum, "A brief intro to metamaterials," IEEE Potentials **23**, 44–46 (2005).

[3] Y. Liu and X. Zhang, "Metamaterials: A new frontier of science and technology," Chem. Soc. Rev. **40**, 2494–2507 (2011).

[4] T. A. M. Hewage, K. L. Alderson, A. Alderson, and F. Scarpa, "Double-negative mechanical metamaterials displaying simultaneous negative stiffness and negative Poisson's ratio properties," Adv. Mater. **28**, 10323–10332 (2016).

[5] J. U. Surjadi, L. Gao, H. Du, X. Li, X. Xiong, N. X. Fang, and Y. Lu, "Mechanical metamaterials and their engineering applications," Adv. Eng. Mater. **21**, 1800864 (2019).

[6] J. Shi and A. H. Akbarzadeh, "Architected cellular piezoelectric metamaterials: Thermo-electro-mechanical properties," Acta Mater. **163**, 91–121 (2019).

[7] X. Yu, J. Zhou, H. Liang, Z. Jiang, and L. Wu, "Mechanical metamaterials associated with stiffness, rigidity and compressibility: A brief review," Prog. Mater. Sci. **94**, 114–173 (2018).

[8] R. D. Kornbluh, H. Prahlad, R. Pelrine, S. Stanford, M. A. Rosenthal, and P. A. von Guggenberg, "Rubber to rigid, clamped to undamped: Toward composite materials with wide-range controllable stiffness and damping," Proc. SPIE **5388**, 372–386 (2004).

[9] B. Haghpanah, H. Ebrahimi, D. Mousanezhad, J. Hopkins, and A. Vaziri, "Programmable elastic metamaterials," Adv. Eng. Mater. **18**, 643–649 (2016).

[10] E. P. Westebring-van der Putten, R. H. M. Goossens, J. J. Jakimowicz, and J. Dankelman, "Haptics in minimally invasive surgery – a review," Minimally Invasive Ther. Allied Technol. **17**, 3–16 (2008).

[11] M. A. Beijen, J. van Dijk, W. B. J. Hakvoort, and M. F. Heertjes, "Self-tuning feedforward control for active vibration isolation of precision machines," IFAC Proc. Vol. **47**, 5611–5616 (2014), part of Special Issue on 19th IFAC World Congress.

[12] *Electroactive Polymer (EAP) Actuators as Artificial Muscles: Reality, Potential, and Challenges*, edited by Y. Bar-Cohen (SPIE Press, 2004), Vol. PM136.

[13] M. Wei, Y. Gao, X. Li, and M. J. Serpe, "Stimuli-responsive polymers and their applications," Polym. Chem. **8**, 127–143 (2017).

[14] W. MohdIsa, A. Hunt, and S. H. HosseinNia, "Sensing and self-sensing actuation methods for ionic polymer-metal composite (IPMC): A review," Sensors **19**, 3967 (2019).

[15] G. Mcknight, R. Doty, A. Keefe, G. Herrera, and C. Henry, "Segmented reinforcement variable stiffness materials for reconfigurable surfaces," J. Intell. Mater. Syst. Struct. **21**, 1783–1793 (2010).

[16] R. Ginés, A. Bergamini, M. Motavalli, and P. Ermanni, "Stiffening and damping capacity of an electrostatically tuneable functional composite cantilever beam," Smart Mater. Struct. **24**, 095008 (2015).

[17] O. Pabst, J. Perelaer, E. Beckert, U. S. Schubert, R. Eberhardt, and A. Tünnermann, "All inkjet-printed piezoelectric polymer actuators: Characterization and applications for micropumps in lab-on-a-chip systems," Org. Electron. **14**, 3423–3429 (2013).

[18] D. Thuau, K. Kallitsis, F. D. Dos Santos, and G. Hadziioannou, "All inkjet-printed piezoelectric electronic devices: Energy generators, sensors and actuators," J. Mater. Chem. C **5**, 9963–9966 (2017).

[19] K. K. Baelz and A. Hunt, "P(VDF-TrFE-CTFE) actuators with inkjet printed electrodes," in *2019 7th International Conference on Control, Mechatronics and Automation (ICCMA)* (IEEE, 2019), pp. 327–332.

[20] S. Xiao, T. Wang, T. Liu, C. Zhou, X. Jiang, and J. Zhang, "Active metamaterials and metadevices: A review," J. Phys. D: Appl. Phys. **53**, 503002 (2020).

[21] R. Poon and J. B. Hopkins, "Phase-changing metamaterial capable of variable stiffness and shape morphing," Adv. Eng. Mater. **21**, 1900802 (2019).

[22] J. T. B. Overvelde, T. A. de Jong, Y. Shevchenko, S. A. Becerra, G. M. Whitesides, J. C. Weaver, C. Hoberman, and K. Bertoldi, "A three-dimensional actuated origami-inspired transformable metamaterial with multiple degrees of freedom," Nat. Commun. **7**, 10929 (2016).

[23] D. Thomas, "Active metamaterials: Unit cells for tunable damping," M.Sc. thesis, Delft University of Technology, Delft, 2020.

[24] See https://www.piezodrive.com/actuators/150v-piezo-stack-actuators-2/ for PiezoDrive "150v piezo stack actuators" (last accessed 12 August 2022).

[25] R. Legtenberg, A. W. Groeneveld, and M. Elwenspoek, "Comb-drive actuators for large displacements," J. Micromech. Microeng. **6**, 320–329 (1996).

[26] H. Conrad, H. Schenk, B. Kaiser, S. Langa, M. Gaudet, K. Schimmanz, M. Stolz, and M. Lenz, "A small-gap electrostatic micro-actuator for large deflections," Nat. Commun. **6**, 10078 (2015).

[27] R. W. Johnstone and M. Parmaswaran, *An Introduction to Surface-Micromachining*, 1st ed. (Springer, New York, 2004).

[28] X. Lv, W. Wei, X. Mao, Y. Chen, J. Yang, and F. Yang, "A novel MEMS electromagnetic actuator with large displacement," Sens. Actuators, A **221**, 22–28 (2015).

[29] R. Munnig Schmidt, G. Schitter, A. Rankers, and J. van Eijk, *The Design of High Performance Mechatronics*, 2nd ed. (IOS Press, Amsterdam, 2014).

[30] J. Hricko and Š. Havlík, "Compliant mechanisms for motion/force amplifiers for robotics," in *Advances in Service and Industrial Robotics* (Springer International Publishing, Cham, 2020), pp. 26–33.

[31] F. Chen, Q. Zhang, Y. Gao, and W. Dong, "A review on the flexure-based displacement amplification mechanisms," IEEE Access **8**, 205919–205937 (2020).

[32] Q. Xu and Y. Li, "Analytical modeling, optimization and testing of a compound bridge-type compliant displacement amplifier," Mech. Mach. Theory **46**, 183–200 (2011).

[33] Y. Li, S. Bi, and C. Zhao, "Analytical modeling and analysis of rhombus-type amplifier based on beam flexures," Mech. Mach. Theory **139**, 195–211 (2019).

[34] See https://www.stratasys.com/en/materials/materials-catalog/polyjet-materials/vero/ for "Vero: Product data sheet for j7 and j8 series" (last accessed 12 August 2022).